

# $W^+W^-$ production at high transverse momenta beyond NLO <sup>☆</sup>

Francisco Campanario <sup>a</sup>, Michael Rauch <sup>b</sup>, Sebastian Sapeta <sup>c,\*</sup>

<sup>a</sup> Theory Division, IFIC, University of Valencia – CSIC, E-46980 Paterna, Valencia, Spain

<sup>b</sup> Institute for Theoretical Physics, Karlsruhe Institute of Technology (KIT), Germany

<sup>c</sup> Institute for Particle Physics Phenomenology, Durham University, South Rd, Durham DH1 3LE, United Kingdom

Received 14 October 2013; received in revised form 28 November 2013; accepted 4 December 2013

Available online 7 December 2013

## Abstract

Pair production of  $W$  gauge bosons is an important process at the LHC entering many experimental analyses, both as background in new-physics searches or Higgs measurements and as signal in precision studies and tests of the Standard Model. Therefore, accurate predictions for this class of processes are of great interest in order to exploit the full potential of LHC measurements. We use the LoopSim method to combine NLO QCD results for  $WW$  and  $WW + \text{jet}$ , as well as the loop-squared gluon-fusion contribution, to obtain approximate NNLO predictions for  $WW$  production. The cross sections are calculated with VBFNLO and include leptonic decays of the  $W$  bosons as well as finite-width and off-shell effects. We find that the size of the additional corrections beyond NLO can be significant and well outside of the NLO error bands given by renormalization and factorization scale variation. Applying a jet veto, we observe further negative corrections at NNLO, which we relate to the presence of large Sudakov logarithms.

© 2013 The Authors. Published by Elsevier B.V. All rights reserved.

## 1. Introduction

The production of two electroweak bosons constitutes an important process at the Large Hadron Collider (LHC), in particular when combined with the leptonic decay modes of the vector

<sup>☆</sup> This is an open-access article distributed under the terms of the Creative Commons Attribution License, which permits unrestricted use, distribution, and reproduction in any medium, provided the original author and source are credited. Funded by SCOAP<sup>3</sup>.

\* Corresponding author.

E-mail addresses: [francisco.campanario@ific.uv.es](mailto:francisco.campanario@ific.uv.es) (F. Campanario), [michael.rauch@kit.edu](mailto:michael.rauch@kit.edu) (M. Rauch), [sebastian.sapeta@durham.ac.uk](mailto:sebastian.sapeta@durham.ac.uk) (S. Sapeta).

bosons. Of particular interest in this class of processes is the production of two opposite-sign  $W$  bosons, which we will consider in this article.

When letting the  $W$  bosons decay leptonically, this process has two charged leptons of opposite sign and either same or different flavor, and two neutrinos in the final state

$$pp \rightarrow W^+W^- + X \rightarrow \ell_1^+ \nu_1 \ell_2^- \bar{\nu}_2 + X. \quad (1)$$

Due to the presence of neutrinos, it is not possible to reconstruct the invariant mass of each individual  $W$  boson. Therefore, this process is an important background for many measurements at the LHC, for example the searches and studies of Higgs bosons, where it forms an irreducible background to the  $WW$  decay mode of the Higgs [1,2]. It is also an important background process to searches for physics beyond the Standard Model (BSM), which often contains a light stable particle that manifests itself as missing transverse energy in the detector [3–5]. But the  $WW$  production is also interesting in its own right, as it allows to test the SM, e.g. when investigating anomalous triple gauge couplings (aTGC), where it allows to put stringent constraints on parameters like  $\Delta g_1^Z$  [6–8].

From the experimental side,  $WW$  production has been measured at the LHC in the 7 TeV run by both ATLAS and CMS experiments [6,7,9,10], and from CMS also first results at 8 TeV, from the 2012 run, with approximately  $5 \text{ fb}^{-1}$  of integrated luminosity, are available [8]. These results are in reasonable agreement with the SM predictions, with both experiments observing slightly more events than expected but still within two standard deviations range.

On the theory side, the next-to-leading order (NLO) QCD corrections for  $WW$  production have been computed in Ref. [11]. These corrections turn out to be large, of the order of 50% at the level of the total cross section for inclusive cuts. This is mainly due to new contributions appearing in the real-emission part, namely gluon-initiated channels. The large size of the gluon parton density functions (PDFs) partly compensates the suppression from the additional power of the strong coupling constant  $\alpha_s$ . Looking at differential distributions, their K-factors, defined as the ratios at NLO over LO, are also sizable and very often phase-space dependent. This means that a simple multiplication of the LO distributions with the K-factor of the integrated result (which is just a single number) will not reproduce the full NLO distribution correctly. Thus, flexible and fast NLO Monte Carlo programs are needed to obtain reliable predictions. Adding soft-gluon resummation of threshold logarithms gives a mild enhancement of the cross section [12]. Work on the full NNLO QCD corrections to  $WW$  production process has only been started [13].

Gluon-initiated contributions [14], with a closed fermion loop, formally appear only at NNLO QCD. They cannot interfere with the tree-level diagrams and therefore enter as one-loop squared diagrams. However, due to the large gluon PDFs, their numerical impact is relevant, giving a contribution at the 10% level in typical Higgs analyses and at the 3–5% level in inclusive searches.

Electro-weak corrections have been reported for on-shell production in Ref. [15]. While their effect is usually small for integrated cross sections, the tails of differential distributions can receive sizable corrections in typical experimental analysis setups.

Results for  $WWj$  at NLO QCD, which provide one-loop real–virtual and double-real contributions to the NNLO corrections for  $WW$  production, have been computed in a series of papers [16]. The integrated corrections to the LO result are typically in the 40% range, while again the tails of differential distributions can show significantly larger K-factors.

NLO QCD corrections to the double real-emission process  $WWjj$  are also available [17]. Here, no new processes open up at higher-order and hence the integrated NLO result shifts by a moderate value of about 10% relative to LO, with a greatly reduced scale uncertainty.

Because the NLO QCD correction to WW production turns out to be large, it is important to assess the size of the NNLO QCD corrections. WWj at NLO QCD provides an essential piece of the WW at NNLO QCD result, accounting for new sub-processes and new topologies appearing for the first time at NNLO. However, this alone is not enough as it misses the 2-loop contributions which are needed to cancel divergencies of the double-real and real–virtual diagrams. Therefore, we use the LoopSim approach [18] to simulate 2-loop contributions to the WW process and combine them with the tree and 1-loop parts from WW and WWj at NLO. As explained in next section, this gives us a dominant part of the NNLO correction for a number of relevant observables.

Very recently, a related study of WW production with 0 and 1-jets in the final state, using a different framework, has been presented in Ref. [19].

The outline of the paper is as follows. In Section 2 we shortly recap the theoretical framework of combining NLO calculations. Then, in Section 3, we define the used model parameters and cuts, which closely follow the experimental analyses. Finally, in Section 4 we present the results of our calculation both for integrated cross sections as well as several important distributions. We close the paper with a brief summary of our findings in Section 5.

## 2. Theoretical framework

To compute approximate NNLO results for WW production, we use the LoopSim approach [18] to merge WW@NLO and WWj@NLO samples obtained with the VBFNLO package [20]. The WWj@NLO result, provided by VBFNLO, constitutes the double-real and real–virtual parts of WW@NNLO. These parts alone are, however, not sufficient as they diverge upon integration over the phase space of the real partons. Those divergences are bound to be canceled, for sufficiently inclusive observables, by the 2-loop virtual correction, following the KLN [21] theorem. Due to this cancellation, it is possible to construct the dominant part of those 2-loop diagrams from their corresponding real emission counterpart using the LoopSim method. Thereby, the singular structure matches exactly the one from real diagrams with higher multiplicity.

LoopSim is based on unitarity and starts from assigning an approximate angular-ordered branching structure to each WWj@NLO event with the help of the Cambridge/Aachen (C/A) [22,23] jet algorithm, with a given radius  $R_{LS}$ . Then, the underlying hard structure of the event is determined and the corresponding particles are marked as “Born”. The number of Born particles is fixed for a given process, and it is given by the number of final state particles at tree level. For simplicity, we combine the neutrino and anti-lepton and construct a virtual  $W^+$  with the four-momentum given by the sum of the two daughter particles, and similarly for  $W^-$ . Therefore, the number of Born particles for WW production is 2. At NNLO, these can be either two vector bosons, a boson and a parton, or two partons.

The remaining particles, which were not marked as “Born”, are then “looped” by finding all possible ways of recombining them with the emitters. In this step, LoopSim generates an approximate set of 1 and 2-loop diagrams with weights equal to  $(-1)^{\text{number of loops}}$  times the weight of the original event. Finally, a double counting between the approximate 1-loop events generated by LoopSim and the exact 1-loop events from the WWj@NLO sample is removed. To distinguish our results, with simulated loops, from the exact ones, we denote the approximate loops by  $\bar{n}$ , as opposed to  $N$  used for exact loops. So, for example,  $\bar{n}$ LO means the correction with simulated 1-loop diagrams, but  $\bar{n}$ NLO is a result with exact 1-loop diagrams and simulated 2-loop contributions.

Note that, because the weights of the loop diagrams produced by LoopSim come from the corresponding real diagrams with higher multiplicity and differ only by the sign, the sum of weights for a set of events generated by LoopSim from a given original event must be zero (see [18] for a detailed explanation). The latter follows from unitarity and means that, for the fully inclusive case, the  $\bar{n}$ NLO integrated cross section is equal to the NLO one. However, because the W bosons are not necessarily identified as “Born” particles, LoopSim will use this type of events to generate new diagrams with simulated W loops that will not contribute to our result, as we require two W bosons in the final state. Similarly, other cuts imposed on leptons, missing energy and jets will spoil the exact real–virtual cancellation outside of the soft or collinear limit, leading to a difference between  $\bar{n}$ NLO and NLO integrated cross sections.

Our approximate  $\bar{n}$ NLO results will have exact tree and 1-loop parts, and the exact singular part of the 2-loop diagrams. Hence, the results will be finite and they will differ from the full NNLO only by the constant terms of the 2-loop contribution. This difference is, however, very small for an observable,  $A$ , that receives significant NLO corrections due to new channels or new topologies

$$\frac{d\sigma^{\bar{n}\text{NLO}}}{dA} - \frac{d\sigma^{\text{NNLO}}}{dA} = \mathcal{O}\left(\alpha_s^2 \frac{d\sigma^{\text{LO}}}{dA}\right). \quad (2)$$

Therefore, for this type of observables, our  $\bar{n}$ NLO result will contain the dominant part of the NNLO prediction for WW production.

One class of uncertainties of the LoopSim method is probed by varying the  $R_{\text{LS}}$  parameter. It accounts for the part of the procedure related to attributing the emission sequence and the underlying hard structure of the events [18]. The smaller the value of  $R_{\text{LS}}$ , the more likely the particles are recombined with the beam, the larger  $R_{\text{LS}}$ , the more likely they are recombined together. The value of  $R_{\text{LS}}$  affects therefore only the wide-angle or hard emissions where the  $ij$  mergings compete with the mergings with the beam. In this study, we use  $R_{\text{LS}} = 1$  and vary it by  $\pm 0.5$ . As we shall see in Section 4, the uncertainty related to  $R_{\text{LS}}$  is smaller than that coming from renormalization and factorization scale variation, except for the very low  $p_T$  region.

In order to make the communication between VBFNLO and LoopSim possible, an interface has been created [24], which is based on the Les Houches Event (LHE) format [25] used to pass the information between the two programs.

### 3. Computational setup

In our calculation, we take as input parameters in the electroweak sector the masses of the W, Z and Higgs boson, and the Fermi constant. The electromagnetic coupling constant and the weak mixing angle are then derived from the above via electro-weak tree-level relations:

$$\begin{aligned} m_Z &= 91.1876 \text{ GeV}, & G_F &= 1.16637 \times 10^{-5} \text{ GeV}^{-2}, \\ m_W &= 80.398 \text{ GeV}, & \alpha_{\text{em}}^{-1} &= 132.3407, \\ m_H &= 126 \text{ GeV}, & \sin^2(\theta_W) &= 0.22265. \end{aligned} \quad (3)$$

Finite-width effects in propagators with massive gauge bosons are taken into account using a modified version [26,27] of the complex-mass scheme [28], where  $\sin^2(\theta_W)$  is kept real. As numerical values, we use  $\Gamma_W = 2.097 \text{ GeV}$  and  $\Gamma_Z = 2.508 \text{ GeV}$ . The effects of external top or bottom quarks are neglected, but their contribution is taken into account in the closed fermion loops appearing in the gluon-fusion part. We use the following values of top and bottom masses

$$m_t = 172.4 \text{ GeV}, \quad m_b = m_b(m_H) = 2.84 \text{ GeV}. \quad (4)$$

We choose the running bottom mass at the Higgs mass as its largest contribution is in the mediation of the effective  $ggH$  coupling, where this choice turns out to be advantageous. Other choices like an on-shell mass lead to cross section changes at the sub-percent level if considering the continuum box part alone, and are a few percent for the full (box + Higgs) gluon-fusion contribution. Hence, the difference is at the per mill level for the cross section of the full process and the exact choice does not play any role. All other quarks are treated as massless and any quark mixing effects are neglected. Regardless of the order, we take the MSTW NNLO 2008 [29] PDF set with  $\alpha_s(m_Z) = 0.11707$ , using the implementation provided by LHAPDF [30]. The final state partons, if any, are clustered with the anti- $k_t$  algorithm [31], with radius  $R = 0.5$ , as implemented in FastJet [32,33].

As the central value for the factorization and renormalization scales we choose

$$\mu_{F,R} = \frac{1}{2} \left( \sum p_{T,\text{partons}} + \sqrt{p_{T,W^+}^2 + m_{W^+}^2} + \sqrt{p_{T,W^-}^2 + m_{W^-}^2} \right), \quad (5)$$

where  $p_{T,W^\pm}$  and  $m_{W^\pm}$  are the transverse momenta and invariant masses of the decaying W bosons, respectively.

In our phenomenological analysis presented in the next section, we include both electron and muon decay channels of the W boson, in both same-flavor,  $e^+e^-$  and  $\mu^+\mu^-$ , and different-flavor,  $e^\pm\mu^\mp$  variants. Our fiducial volume matches to a large extent that chosen by the CMS experiment in Ref. [8]. The ATLAS setup is also very similar, although the exact numerical values of the cuts differ [6,9].

All events are required to have a pair of oppositely charged leptons of either the first or the second generation (same-flavor case) or one from the first and one from the second generation (different-flavor). Both of them must fulfill the cuts

$$p_{T,\ell} > 20 \text{ GeV} \quad \text{and} \quad |\eta_\ell| < 2.5. \quad (6)$$

A *projected*  $E_{T,\text{miss}}$  is defined, following Ref. [8], as the missing transverse energy, if the angle between the missing transverse momentum and the lepton closest in azimuthal angle is larger than  $\pi/2$ , or its component transverse to the closest lepton direction otherwise. For different-flavor configurations, we require that the *projected*  $E_{T,\text{miss}} > 20 \text{ GeV}$ .

In the same-flavor case, we use a more restrictive cut with *projected*  $E_{T,\text{miss}} > 45 \text{ GeV}$ . Moreover, we select only events with dilepton mass  $m_{\ell\ell} > 12 \text{ GeV}$ ,  $|m_{\ell\ell} - m_Z| > 15 \text{ GeV}$  and dilepton transverse momentum  $p_{T,\ell\ell} > 45 \text{ GeV}$ . For these same-flavor runs, we also require that the angle in the transverse plane between the dilepton system and the most energetic jet with  $p_T > 15 \text{ GeV}$  is smaller than 165 degrees. These additional dilepton cuts are used by the experiments to reduce Drell–Yan background and jets misidentified as leptons.

In our study, we shall discuss two classes of results – without and with jet veto. For the latter case, we reject all events containing one or more jets with  $p_{T,\text{jet}} > 30 \text{ GeV}$  and  $|\eta_{\text{jet}}| < 4.7$ . These vetoed results are particularly important when discussing the impact of our findings on the experimental results. The measurements of the inclusive WW cross section by both ATLAS and CMS have been performed with a vetoed setup [6–10]. Also in the studies and searches of the Higgs boson, events are grouped into categories with different jet multiplicity. For the lowest 0-jet bin this effectively corresponds to a jet veto, and for higher ones correspondingly to  $n$ -jet exclusive samples with vetoes on additional jets beyond the desired number [1,2]. As we shall see in the following section, these two classes of results exhibit distinctly different behavior of higher order perturbative QCD corrections.

#### 4. Numerical results

In [Table 1](#), we present numerical results for integrated cross sections. All results correspond to the LHC with a center-of-mass energy  $\sqrt{s} = 8$  TeV and are summed over same and different-flavor combinations in the final state. We adopt the convention according to which  $\sigma_{\text{NLO}}$  and  $\sigma_{\bar{n}\text{NLO}}$ , given in the last two rows of [Table 1](#), contain also the gluon-fusion contribution (“box + Higgs”). Pure NLO and  $\bar{n}\text{NLO}$  cross sections (labeled pure-NLO and pure- $\bar{n}\text{NLO}$ ) are given in the 3rd and the 4th row of [Table 1](#), respectively. The uncertainties are obtained by varying the renormalization and factorization scale  $\mu_R = \mu_F = \mu$  by the factors  $2^{\pm 1}$ . For the  $\bar{n}\text{NLO}$  cross sections, we also give the errors from changing the radius parameter  $R_{\text{LS}}$  to 0.5 and 1.5. The scale uncertainties of the NLO ( $\bar{n}\text{NLO}$ ) cross sections were obtained by linearly adding the uncertainties of the pure-NLO (pure- $\bar{n}\text{NLO}$ ) and the box + Higgs contributions (see discussion below).

The central column of [Table 1](#) shows the integrated cross sections without imposing any cuts on additional jets. Going from LO to pure-NLO, we observe corrections of the order of 35%. The scale uncertainty is marginally reduced from a little bit above 2% at LO to a little bit below 2% at pure-NLO. Merging the NLO results for WW and WWj with LoopSim gives the pure- $\bar{n}\text{NLO}$  cross section, which in the case without jet veto is about 3% higher than pure-NLO. The scale uncertainty is at the similar 2% level. On top of that, the uncertainty due to  $R_{\text{LS}}$  variation is about 1.5%.

In the lower part of [Table 1](#) we show the NLO and  $\bar{n}\text{NLO}$  cross sections, which include the loop-squared gluon-fusion box and Higgs contributions. The scale uncertainties were obtained by linearly adding the respective positive and negative uncertainties of the pure-NLO (pure- $\bar{n}\text{NLO}$ ) and the box + Higgs parts. Even though the box + Higgs contributes only about 5% to the NLO and  $\bar{n}\text{NLO}$  results, it comes with a relatively large scale uncertainty of 25% of the box + Higgs cross section. This is because the gluon-fusion contribution is effectively of leading order type as it enters for the first time at  $\mathcal{O}(\alpha_{\text{EW}}^2 \alpha_s^2)$ . Altogether, the scale uncertainties of  $\sigma_{\text{NLO}}$  and  $\sigma_{\bar{n}\text{NLO}}$  are at the level of 3%.

The right column of [Table 1](#) shows the values of the cross sections when a jet veto is imposed. The LO and box + Higgs results obviously do not differ from the non-veto case as they have no partons in the final state. The K-factor from LO to pure-NLO is at the level of 2.5%, much smaller than in the case without veto. The scale uncertainty reduces by 40%. Going one order higher, it turns out that the  $\mathcal{O}(\alpha_{\text{EW}}^2 \alpha_s^2)$  corrections are negative and therefore the cross section decreases at pure- $\bar{n}\text{NLO}$ . It also yields a reduced scale uncertainty below 1%. Hence, even if we combine it with the  $R_{\text{LS}}$  error, the pure- $\bar{n}\text{NLO}$  result in the vetoed case is still well below that at pure-NLO.

We mentioned earlier that the uncertainties of the full NLO and  $\bar{n}\text{NLO}$  (hence with box + Higgs) were obtained by linearly adding individual errors of each contribution. We choose this procedure since a naive scale variation of the sum of pure-NLO and box + Higgs, for the case with jet veto, gives a nearly vanishing scale uncertainty of  $\sigma_{\text{NLO}}$ , which is a result of an accidental cancellation between the pure NLO part and the gluon-fusion part. That, in turn, is due to the fact that  $\sigma_{\text{pure-NLO}}$  is an increasing, while  $\sigma_{\text{box+Higgs}}$  is a decreasing function of  $\mu$ . Therefore they compensate each other in the sum, which changes only by  ${}_{+0.10}^{-0.72}$  upon scale variation. We believe that adding errors of each individual contribution linearly gives a much more realistic estimate of the uncertainty. In all other cases, i.e. pure- $\bar{n}\text{NLO}$  with veto and pure-NLO and pure- $\bar{n}\text{NLO}$  without veto, the cross section decreases as function of  $\mu$ , just like in the box + Higgs part. Hence, for those results, adding the errors linearly is equivalent to the naive scale variation. Therefore, our procedure can be used across all results given in [Table 1](#).

Table 1

Integrated (fiducial) cross sections for  $pp \rightarrow W^+W^- \rightarrow \ell^+ \nu \ell^- \bar{\nu}$  at the LHC with  $\sqrt{s} = 8$  TeV using the parameter settings and cuts given in Section 3. According to the naming convention adopted throughout the paper,  $\sigma_{\text{NLO}}$  and  $\sigma_{\bar{n}\text{NLO}}$ , given in the last two rows, contain the gluon-fusion contribution (labeled “box + Higgs” above). Pure NLO and  $\bar{n}\text{NLO}$  cross sections (labeled with pure-NLO and pure- $\bar{n}\text{NLO}$ ) are given in the 3rd and the 4th row, respectively. For the upper part of the table, the values in superscript correspond to the renormalization and factorization scale  $\mu = 2\mu_0$ , whereas those in subscript refer to  $\mu = \frac{1}{2}\mu_0$ . Similarly, for the  $\bar{n}\text{NLO}$  results, we give the cross sections for the  $R = 1.5$  and  $R = 0.5$  choices (each time with the central scale  $\mu_0$ ) in the upper and lower case, respectively. The scale uncertainties of the NLO ( $\bar{n}\text{NLO}$ ) cross sections, shown in the lower part of the table, were obtained by linearly adding the respective positive and negative uncertainties of the pure-NLO (pure- $\bar{n}\text{NLO}$ ) and the box + Higgs contributions (see text for details). The statistical error from Monte Carlo integration is at the per mill level for all results.

	c.s. [fb] without jet veto		c.s. [fb] with jet veto	
$\sigma_{\text{LO}}$	247.49 <sup>+5.40</sup> <sub>-7.60</sub>		247.49 <sup>+5.40</sup> <sub>-7.60</sub>	
$\sigma_{\text{box+Higgs}}$	19.02 <sup>-3.70</sup> <sub>+4.86</sub>		19.02 <sup>-3.70</sup> <sub>+4.86</sub>	
$\sigma_{\text{pure-NLO}}$	334.64 <sup>-6.36</sup> <sub>+6.49</sub>		253.05 <sup>+2.98</sup> <sub>-4.75</sub>	
$\sigma_{\text{pure-}\bar{n}\text{NLO}}$	345.17 <sup>-7.06</sup> <sub>+7.03</sub> ( $\mu$ )	<sup>+5.24</sup> <sub>-3.33</sub> ( $R_{\text{LS}}$ )	236.63 <sup>-1.16</sup> <sub>+1.45</sub> ( $\mu$ )	<sup>+5.31</sup> <sub>-3.27</sub> ( $R_{\text{LS}}$ )
$\sigma_{\text{NLO}}$	353.67 <sup>-10.06</sup> <sub>+11.35</sub>		272.07 <sup>-8.45</sup> <sub>+7.84</sub>	
$\sigma_{\bar{n}\text{NLO}}$	364.19 <sup>-10.76</sup> <sub>+11.89</sub> ( $\mu$ )	<sup>+5.24</sup> <sub>-3.33</sub> ( $R_{\text{LS}}$ )	255.72 <sup>-4.86</sup> <sub>+6.31</sub> ( $\mu$ )	<sup>+5.31</sup> <sub>-3.27</sub> ( $R_{\text{LS}}$ )

Finally, let us mention that the LoopSim method was designed to give an accurate estimate of the NNLO result predominantly at high- $p_T$ , where the constant term of 2-loop diagrams is of less importance. This constant term can however bring significant contributions to the total cross section. Therefore, the  $\bar{n}\text{NLO}$  result for the integrated (fiducial) cross section, presented in Table 1, captures the exact logarithmic terms of NNLO, but only part of the constant terms, namely those coming from the tree and 1-loop diagrams. We believe that this adds additional information as it includes, for instance, the contributions from new partonic channels. One should however still expect a genuine 2-loop correction on top of the numbers given in Table 1.

In Figs. 1–5 we then present several differential distributions. On the left-hand side of each figure we show cross sections without cuts on possible final-state jets, while on the right-hand side, additionally a jet veto is imposed. The upper panel of each graph shows various differential cross sections. The NLO and  $\bar{n}\text{NLO}$  curves both include the contribution from the gluon-fusion diagrams, which is also shown separately with label “box + Higgs”. The cyan “ $\bar{n}\text{NLO}$  ( $R_{\text{LS}}$ )” band shows the uncertainty from varying the LoopSim parameter, whereas all other bands denote the change from varying the scale by a factor  $2^{\pm 1}$ . For the results with the gluon-fusion part, i.e. NLO and  $\bar{n}\text{NLO}$ , the width of the band corresponds to linearly adding errors. In the middle and the bottom panels we plot the differential K-factor with respect to LO and NLO, respectively,

$$K_{\text{LO}} = \frac{d\sigma/dx}{d\sigma_{\text{LO}}/dx}, \quad K_{\text{NLO}} = \frac{d\sigma/dx}{d\sigma_{\text{NLO}}/dx}. \quad (7)$$

The NLO curve also includes the gluon-fusion contribution.

In Fig. 1 we show the effective mass observable  $H_T$ , defined as

$$H_T = \sum p_{T,\text{jets}} + \sum p_{T,\ell} + E_{T,\text{miss}}, \quad (8)$$

which is commonly used in new-physics searches. This variable is very sensitive to additional radiation from further partons and soft or collinear emission of the W bosons. Once the former pass certain transverse momenta and emission angles, they yield a significant enhancement of



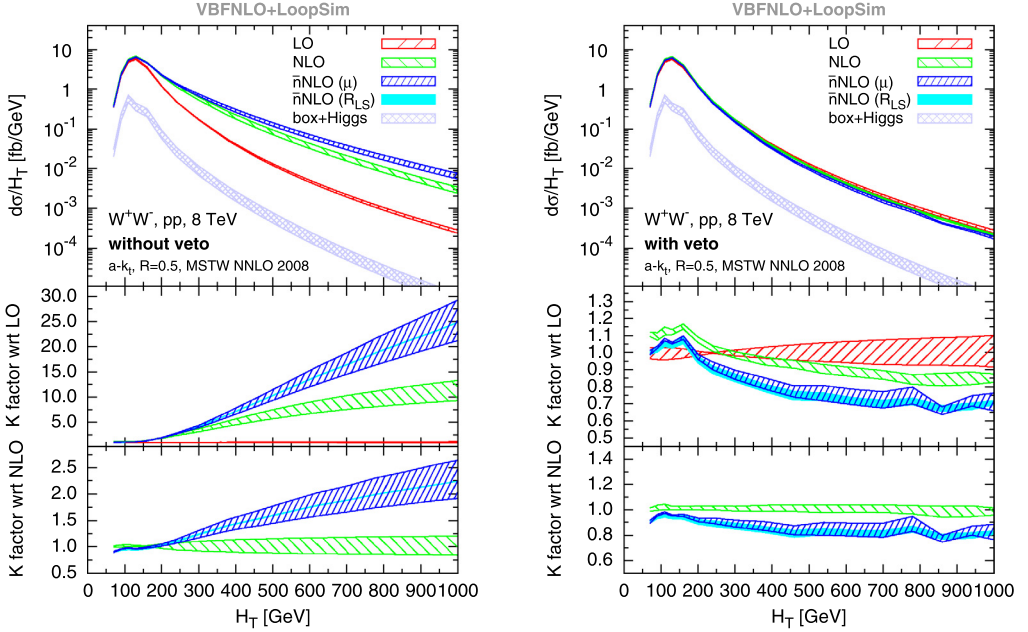


Fig. 1. Differential cross sections and K-factors for the effective mass observable, defined in Eq. (8), for the LHC at  $\sqrt{s} = 8$  TeV. The bands correspond to varying  $\mu_F = \mu_R \equiv \mu$  by factors 1/2 and 2 around the central value from Eq. (5). The cyan solid bands give the uncertainty related to the  $R_{LS}$  parameter varied between 0.5 and 1.5. The distribution is a sum of contributions from  $e^+v_e e^- \bar{\nu}_e$ ,  $\mu^+v_\mu \mu^- \bar{\nu}_\mu$ ,  $e^+v_e \mu^- \bar{\nu}_\mu$  and  $\mu^+v_\mu e^- \bar{\nu}_e$  decay channels. The contribution from the gluon-fusion box and Higgs diagrams is included in the NLO and  $\bar{n}$ NLO curves. The left panels correspond to the inclusive sample, while the results shown in the right panel were obtained with vetoing events containing jets which fulfill the criteria  $p_{T,jet} > 30$  GeV and  $|\eta_{jet}| < 4.7$ . (For interpretation of the references to color in this figure, the reader is referred to the web version of this article.)

the differential distribution of  $H_T$ . Therefore one expects that without jet veto one observes large K-factors in the high  $H_T$  range. This is indeed seen on the left-hand side of Fig. 1. For small values of  $H_T$ , both K-factors are close to unity. Around a few hundred GeV, however, the K-factors become huge, with values of  $K_{LO}$  reaching 12 for NLO and 25 for  $\bar{n}$ NLO at 1 TeV and still a factor two for the  $\bar{n}$ NLO/NLO K-factor. We have also checked that for all distributions that exhibit a large K-factor, discussed in this paper, the  $\bar{n}$ LO result is very close to NLO at  $p_T$  above 200 GeV.

The situation is completely different when we switch on the jet veto. For small  $H_T$  values, the K-factor is again small, but at high  $H_T$ , the differential cross section gets significantly reduced as we go from LO to NLO and from NLO to  $\bar{n}$ NLO. This can be easily understood from the definition of  $H_T$ . An additional splitting which leads to a further final-state jet will increase  $H_T$  while leaving the partonic center-of-mass energy invariant. Hence, there are proportionally more events with additional jets at large  $H_T$  values. By imposing the jet veto, we remove those events and therefore kill the huge K-factor seen in the unvetted plots on the left. On top of that, the jet veto procedure introduces Sudakov-type logarithms by forbidding radiation in certain regions of phase space. These logarithms bring negative corrections to the cross section at high  $H_T$ . This is precisely what we observe in the K-factor plots on the right-hand side of Fig. 1. The NLO/LO and  $\bar{n}$ NLO/LO K-factors rise a little for small  $H_T$ , where the impact of the jet veto is still small.



For slightly higher  $H_T$ , however, the restriction of additional radiation leads to suppression and eventually fairly rapid drop of the K-factors.

The cyan solid bands in Fig. 1 show the uncertainty due to varying the  $R_{LS}$  parameter (related to attributing emission sequence and hard structure of the events, as explained in Section 2). For the vetoed result, this is already smaller than the scale dependence at  $\bar{n}$ NLO, while in the unvetoed case this uncertainty is completely negligible.

All in all, the  $\bar{n}$ NLO QCD turns out to bring further negative corrections to  $H_T$  above about 200 GeV for the case with jet veto. One should however be careful while interpreting these results. On one hand, they are potentially subject to further corrections from the constant term of 2-loop diagrams.<sup>1</sup> These effects are not accounted for by the  $R_{LS}$  uncertainty band. On the other hand, the non-negligible NLO correction at high  $H_T$  suggests that the Sudakov logarithms are relevant. Our  $\bar{n}$ NLO result provides these type of logarithmic contributions one order higher, hence it supplements the NLO with an important part of the genuine NNLO correction. To what extent this negative, Sudakov-type correction is counterbalanced by the finite terms, can only be checked by performing the full NNLO calculation. Our approximate  $\bar{n}$ NLO result for the vetoed case gives already some indications and an insight into what happens at  $\mathcal{O}(\alpha_{EW}^2\alpha_s^2)$ . Moreover, as shown in the following figures, it demonstrates that the small scale uncertainty of many of the NLO results with jet veto is to a large extent accidental, as the corresponding uncertainty at  $\bar{n}$ NLO comes out larger than that of NLO.

Fig. 2 shows another important variable, the transverse momentum of the hardest lepton,  $p_{T,\ell,\max}$ , which is extensively used in the studies of anomalous triple gauge couplings. Let us first consider the unvetoed results shown on the left-hand side. For small transverse momenta, where the bulk of the cross section lies, the differential NLO K-factor is close to the integrated one. It then rises when we go to larger  $p_{T,\ell,\max}$  values and finally, above 300 GeV, reaches a plateau at a value of around 2.5. The additional  $\bar{n}$ NLO corrections are very small at the lower boundary, but they grow to an additional 20% contribution at large values. Thereby, the NLO and  $\bar{n}$ NLO scale variation bands barely overlap, while the uncertainty from  $R_{LS}$  variation is very small. For the actual anomalous gauge coupling searches, an additional jet veto is imposed to remove events where the whole WW system recoils against jets, which yield only low sensitivity to aTGC effects. Looking at the vetoed results, shown on the right-hand side of Fig. 2, we observe that, at large transverse momenta, the NLO cross section, including the gluon-fusion contribution, is about 15% smaller than LO. The  $\bar{n}$ NLO correction brings an additional reduction compared to NLO by roughly the same amount. Moreover, the scale uncertainty at  $\bar{n}$ NLO is bigger than at NLO, indicating that the seemingly small error of the NLO result is largely accidental. Also here the uncertainty due to varying  $R_{LS}$  is smaller than the scale uncertainty. Hence, the additional contribution from the NLO calculation of WWj leads to a further reduction of the cross section.

Another interesting observable is the missing transverse energy,  $E_{T,\text{miss}}$ , which, again, plays an important role in new physics searches. Most of the BSM models contain a stable, weakly-interacting particle, which manifests itself in the detector as a deficit in transverse energy. In the SM backgrounds, like WW, this deficit is generated by two neutrinos in the final state. In Fig. 3 we present the corresponding distribution of missing  $E_T$ . Expectedly, the behavior is similar

<sup>1</sup> Given that the NLO correction to the inclusive cross section, which comes predominantly from the constant piece of 1-loop diagrams, is  $\mathcal{O}(30\%)$ , a similar correction from the finite term of 2-loop diagrams could be naively estimated as a square of the 1-loop term, hence it would amount to  $\mathcal{O}(10\%)$ .

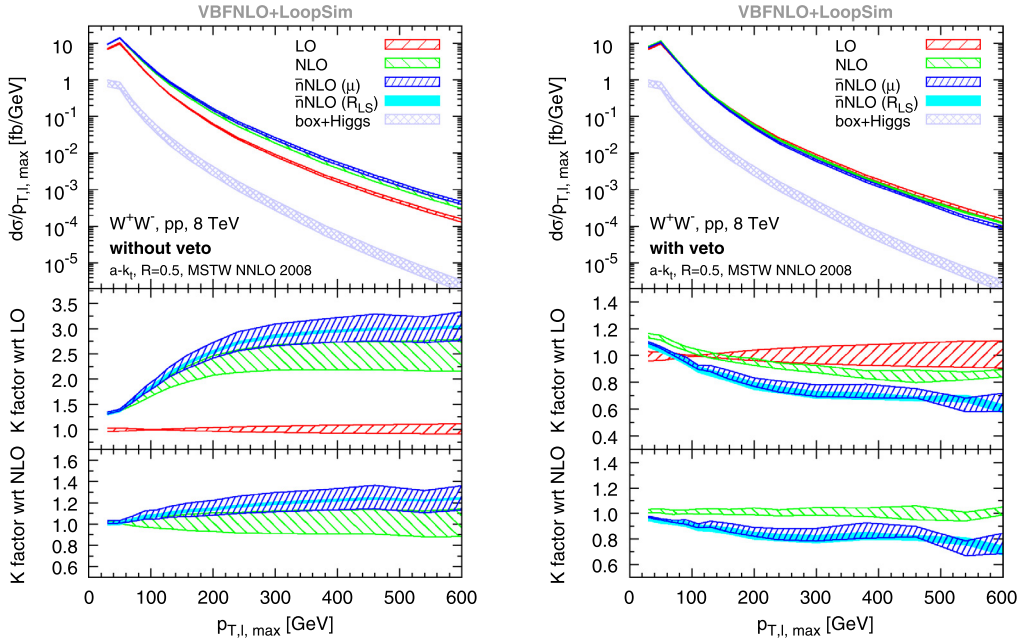


Fig. 2. Differential cross sections and K-factors for the  $p_T$  of the hardest lepton for the LHC at  $\sqrt{s} = 8$  TeV without (left) and with jet veto (right). Details are as in Fig. 1.

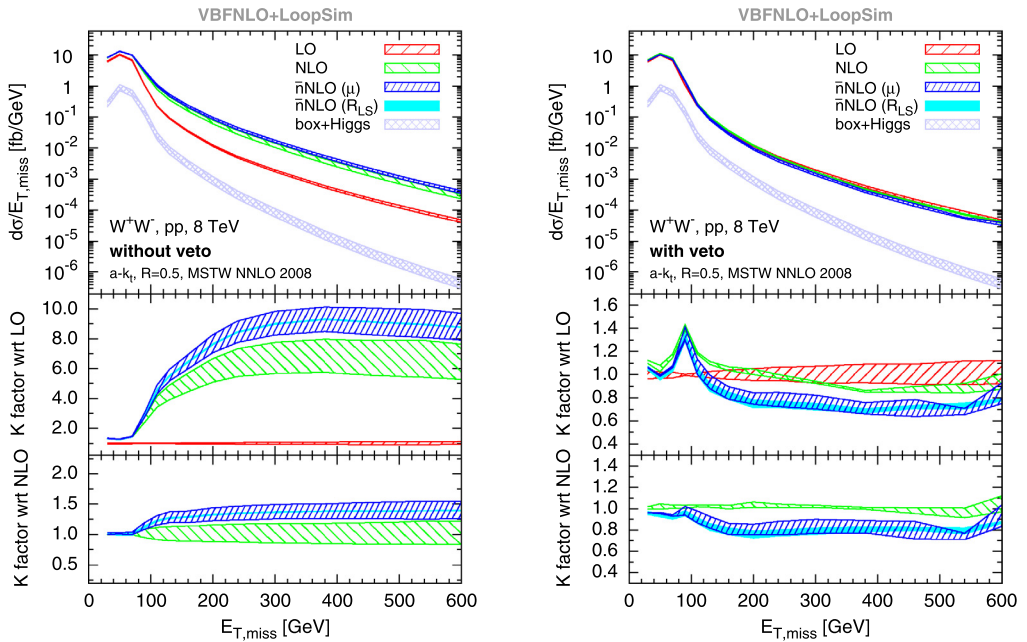


Fig. 3. Differential cross sections and K-factors for the missing transverse energy for the LHC at  $\sqrt{s} = 8$  TeV without (left) and with jet veto (right). Details are as in Fig. 1.

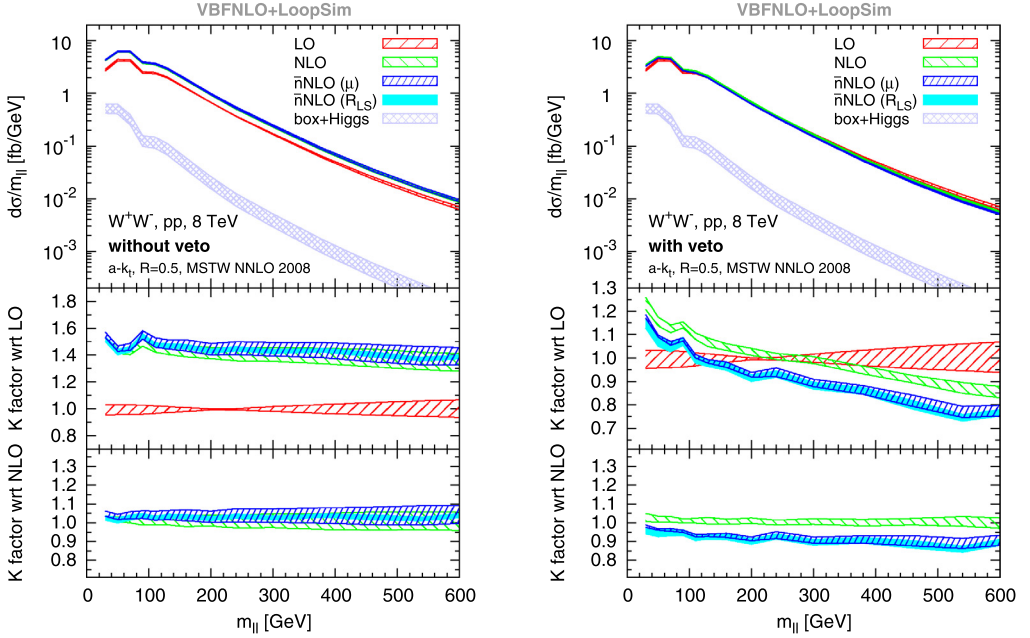


Fig. 4. Differential cross sections and K-factors for the invariant mass of the dilepton system for the LHC at  $\sqrt{s} = 8$  TeV without (left) and with jet veto (right). Details are as in Fig. 1.

to that of the lepton's transverse momentum shown in the previous figure. The size of the corrections, however, is even larger here. For the unvetoesd cross sections, the NLO/LO K-factor reaches up to 7 at 600 GeV and the  $\bar{n}$ NLO contribution gives an additional 30%. Again, the latter is outside the NLO scale variation bands, while the  $R_{LS}$  variation is small. The vetoed results, in contrast, show a decrease of the cross section at larger missing transverse energy. Thereby, the scale variation uncertainties from NLO and  $\bar{n}$ NLO do not overlap, and the latter is still larger than the  $R_{LS}$  error. The peak in the NLO/LO and  $\bar{n}$ NLO/LO K-factors has the same origins as a similar peak in the  $H_T$  distribution discussed above. The strong growth at low  $E_{T,miss}$  is just the remnant of the large K-factor from the left plot, in the region where the impact of jet veto is still limited. Then, around 100 GeV, large negative logarithmic corrections from the veto take over and the K-factor starts decreasing. Similarly to the  $p_{T,\ell,max}$  case, the scale uncertainty of the  $\bar{n}$ NLO vetoed result is larger than that at NLO due to accidental cancellations occurring in the latter.

In Fig. 4 we show the invariant mass of the dilepton system. This variable plays a crucial role in separating the signal and the control regions of the WW background in Higgs measurements, although the relevant energy range there is smaller than the one shown here. For the unvetoesd results, we observe a significant correction similar to the integrated one when going to NLO, which is basically constant in  $m_{\ell\ell}$ . The additional  $\bar{n}$ NLO corrections, on the other hand, are small and well within the scale variation uncertainties. This happens because the distribution from Fig. 4 in the high  $m_{\ell\ell}$  region, where configurations with back-to-back leptons dominate, is not particularly sensitive to new topologies, and the finite terms from the two-loop diagrams, which are missing in the  $\bar{n}$ NLO result, are of larger relative importance for this observable. The dip in the cross section around the Z boson mass is caused by the cut on this variable in the same-flavor case.

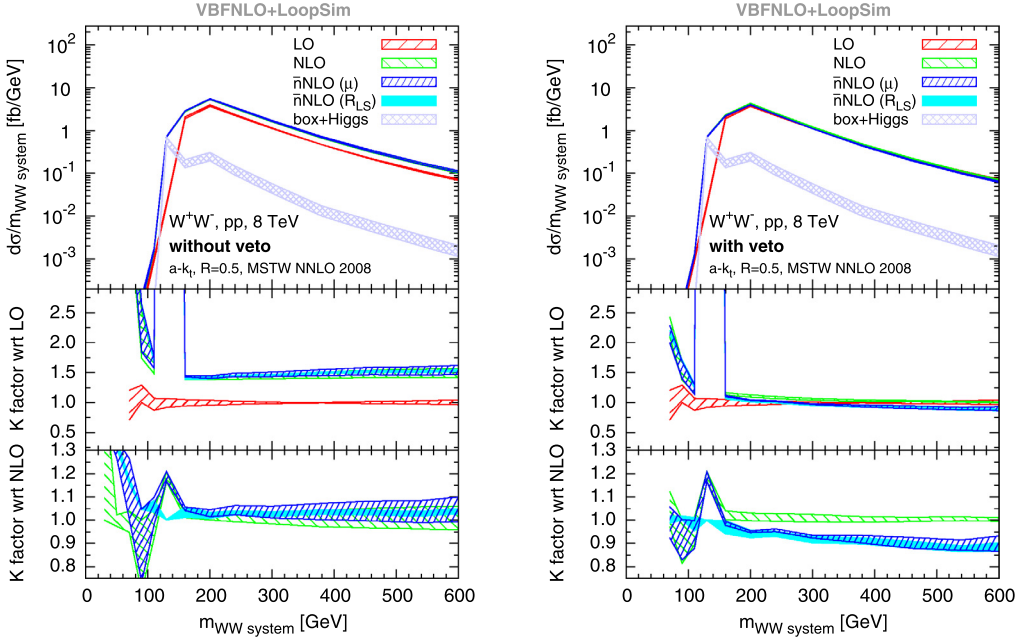


Fig. 5. Differential cross sections and K-factors for the invariant mass of the diboson system for the LHC at  $\sqrt{s} = 8$  TeV without (left) and with jet veto (right). Details are as in Fig. 1.

The results with jet veto show a different behavior. The NLO/LO K-factor clearly exhibits a non-constant shape, with positive corrections of about 15% at the lower boundary, which gradually falls to negative corrections by over 20% at the upper end of the shown range. When going to  $\bar{n}$ NLO, we always observe a negative correction, which gradually increases in the plotted range. Thereby, only at very small values the scale uncertainty bands of NLO and  $\bar{n}$ NLO overlap, while at larger values the corrections are clearly stronger. The uncertainty from the  $R_{LS}$  variation is in the same range as the  $\bar{n}$ NLO scale error.

Finally, in Fig. 5 the invariant mass of the WW system is plotted and shows several interesting features. At 126 GeV, in the gluon-fusion curve, and hence in the NLO and  $\bar{n}$ NLO ones, which include this contribution, the peak from the s-channel Higgs boson is clearly visible. Then, these cross sections drop again, before, at twice the W mass, continuum production opens up, which is also present in the LO curve. Looking at the K-factors, in the unvetoeed case, we see significant effects from NLO QCD corrections and the loop-induced gluon-fusion contribution. Beyond that, the additional  $\bar{n}$ NLO contributions are well covered by the NLO scale variation for similar reasons as in the  $m_{\ell\ell}$  case discussed above. The distributions with jet veto, depicted in Fig. 5 (right), show two distinct regions. Roughly below the WW threshold, we observe the expected large effects for the K-factor with respect to LO due to the gluon-fusion contribution, while the  $\bar{n}$ NLO effects are small. Above this value, the NLO corrections become gradually smaller and in the high-energy range are well within the LO scale variation. The  $\bar{n}$ NLO part, on the other hand, gives a gradually growing negative contribution, raising up to about 10% of NLO, which is greater than the bands given by scale uncertainties and the band due the  $R_{LS}$  variation.

## 5. Conclusions

In this article, we have considered WW diboson production beyond NLO with W bosons decaying leptonically. This process is an important background for many new-physics searches as well as SM processes like the Higgs boson measurements. Furthermore, it is also important as a signal process for measuring anomalous triple gauge couplings. The NLO QCD calculations of WW and WW + jet production, as well as the loop-induced gluon-fusion contribution, implemented in VBFNLO, have been merged using the LoopSim method to obtain approximate NNLO results for WW production. The cuts followed closely those used by the two LHC experiments.

For observables which are sensitive to QCD radiation, like  $H_T$  or the transverse momentum of the leading lepton, we find large additional corrections beyond NLO. These are typically outside the NLO error bands given by a scale variation of a factor  $\frac{1}{2}$  and 2. The invariant-mass distributions of the dilepton and diboson system, on the other hand, do not receive significant  $\bar{n}$ NLO corrections.

Once we impose a veto on jets, as is typically done in the experimental analyses, we observe further significant negative corrections beyond the NLO prediction in the high-energy range above approximately 150 GeV, which can be explained by the appearance of large Sudakov logarithms. Their size is larger than the error estimate given by a scale variation of the NLO cross section and the scale uncertainty of the  $\bar{n}$ NLO result itself is larger than that of NLO, which points to an accidental cancellation occurring in the latter. The  $\bar{n}$ NLO vetoed distributions are also potentially subject to non-negligible corrections from the constant term of the 2-loop diagrams. Uncertainties due to the LoopSim method, which are estimated by varying the  $R_{LS}$  parameter, are always smaller than the remaining scale uncertainties. Therefore, we conclude that the QCD corrections to WW production beyond NLO play an important role for a number of experimentally relevant observables and should be taken into account in the analyses that use WW theory results as an input. Until a full NNLO calculation of WW production is available as Monte Carlo program, our method allows for an inclusion of the dominant part of these effects.

The additions to the VBFNLO program used in this article are available from the authors on request and will be part of a future release. The LoopSim library, together with the Les Houches Event interface, is publicly available at <https://loopsim.hepforge.org>.

## Acknowledgements

We thank Gavin Salam for numerous valuable discussions during all stages of this work and for useful comments on the manuscript. F.C. is funded by a Marie Curie fellowship (PIEF-GA-2011-298960) and partially by MINECO (FPA2011-23596) and by LHCPHENONET (PITN-GA-2010-264564). M.R. acknowledges partial support by the Deutsche Forschungsgemeinschaft via the Sonderforschungsbereich/Transregio SFB/TR-9 “Computational Particle Physics” and the Initiative and Networking Fund of the Helmholtz Association, contract HA-101 (“Physics at the Terascale”).

## References

- [1] G. Aad, et al., ATLAS Collaboration, Phys. Lett. B 716 (2012) 1, arXiv:1207.7214 [hep-ex];  
 G. Aad, et al., ATLAS Collaboration, Phys. Lett. B (2013), arXiv:1307.1427 [hep-ex];  
 G. Aad, et al., ATLAS Collaboration, ATLAS-CONF-2013-030;

- G. Aad, et al., ATLAS Collaboration, ATLAS-CONF-2013-031;  
G. Aad, et al., ATLAS Collaboration, ATLAS-CONF-2013-067.
- [2] S. Chatrchyan, et al., CMS Collaboration, J. High Energy Phys. 1306 (2013) 081, arXiv:1303.4571 [hep-ex];  
S. Chatrchyan, et al., CMS Collaboration, Eur. Phys. J. C 73 (2013) 2469, arXiv:1304.0213 [hep-ex];  
S. Chatrchyan, et al., CMS Collaboration, CMS-PAS-HIG-13-003, CMS-PAS-HIG-13-008.
- [3] B. Feigl, H. Rzehak, D. Zeppenfeld, Phys. Lett. B 717 (2012) 390, arXiv:1205.3468 [hep-ph].
- [4] D. Curtin, P. Jaiswal, P. Meade, Phys. Rev. D 87 (3) (2013) 031701, arXiv:1206.6888 [hep-ph].
- [5] G. Aad, et al., ATLAS Collaboration, Phys. Lett. B 718 (2013) 860, arXiv:1208.2880 [hep-ex].
- [6] G. Aad, et al., ATLAS Collaboration, Phys. Rev. D 87 (2013) 112001, arXiv:1210.2979 [hep-ex].
- [7] S. Chatrchyan, et al., CMS Collaboration, arXiv:1306.1126 [hep-ex].
- [8] S. Chatrchyan, et al., CMS Collaboration, Phys. Lett. B 721 (2013) 190, arXiv:1301.4698 [hep-ex].
- [9] G. Aad, et al., ATLAS Collaboration, Phys. Lett. B 712 (2012) 289, arXiv:1203.6232 [hep-ex].
- [10] S. Chatrchyan, et al., CMS Collaboration, Phys. Lett. B 699 (2011) 25, arXiv:1102.5429 [hep-ex].
- [11] L.J. Dixon, Z. Kunszt, A. Signer, Nucl. Phys. B 531 (1998) 3–23, arXiv:hep-ph/9803250;  
L.J. Dixon, Z. Kunszt, A. Signer, Phys. Rev. D 60 (1999) 114037, arXiv:hep-ph/9907305;  
For updated phenomenological studies see e.g. J.M. Campbell, R.K. Ellis, C. Williams, J. High Energy Phys. 1107 (2011) 018, arXiv:1105.0020 [hep-ph];  
J.M. Campbell, R.K. Ellis, C. Williams, J. High Energy Phys. 1110 (2011) 005, arXiv:1107.5569 [hep-ph].
- [12] S. Dawson, I.M. Lewis, M. Zeng, arXiv:1307.3249 [hep-ph].
- [13] T. Gehrmann, L. Tancredi, E. Weihs, J. High Energy Phys. 1308 (2013) 070, arXiv:1306.6344 [hep-ph];  
G. Chachamis, PoS RADCOR 2009 (2010) 059.
- [14] L. Ametller, E. Gava, N. Paver, D. Treleani, Phys. Rev. D 32 (1985) 1699;  
D.A. Dicus, C. Kao, W. Repko, Phys. Rev. D 36 (1987) 1570;  
E. Glover, J. van der Bij, Phys. Lett. B 219 (1989) 488;  
T. Binoth, M. Ciccolini, N. Kauer, M. Kramer, J. High Energy Phys. 0503 (2005);  
T. Binoth, M. Ciccolini, N. Kauer, M. Kramer, J. High Energy Phys. 0612 (2006) 046;  
M. Bonvini, F. Caola, S. Forte, K. Melnikov, G. Ridolfi, Phys. Rev. D 88 (2013) 034032, arXiv:1304.3053 [hep-ph].
- [15] A. Bierweiler, T. Kasprzik, H. Kuhn, S. Uccirati, J. High Energy Phys. 1211 (2012) 093, arXiv:1208.3147 [hep-ph];  
J. Baglio, L.D. Ninh, M.M. Weber, arXiv:1307.4331 [hep-ph].
- [16] S. Dittmaier, S. Kallweit, P. Uwer, Phys. Rev. Lett. 100 (2008) 062003;  
S. Dittmaier, S. Kallweit, P. Uwer, Nucl. Phys. B 826 (2010) 18;  
T. Melia, K. Melnikov, R. Rontsch, M. Schulze, G. Zanderighi, J. High Energy Phys. 1208 (2012) 115, arXiv:1205.6987 [hep-ph].
- [17] N. Greiner, G. Heinrich, P. Mastrolia, G. Ossola, T. Reiter, F. Tramontano, Phys. Lett. B 713 (2012) 277, arXiv:1202.6004 [hep-ph].
- [18] M. Rubin, G.P. Salam, S. Sapeta, J. High Energy Phys. 1009 (2010) 084.
- [19] F. Cascioli, S. Hoeche, F. Krauss, P. Maierhofer, S. Pozzorini, F. Siegert, arXiv:1309.0500 [hep-ph].
- [20] K. Arnold, M. Bahr, G. Bozzi, F. Campanario, C. Englert, T. Figy, N. Greiner, C. Hackstein, et al., Comput. Phys. Commun. 180 (2009) 1661, arXiv:0811.4559 [hep-ph];  
K. Arnold, J. Bellm, G. Bozzi, M. Brieg, F. Campanario, C. Englert, B. Feigl, J. Frank, et al., arXiv:1107.4038 [hep-ph];  
K. Arnold, J. Bellm, G. Bozzi, F. Campanario, C. Englert, B. Feigl, J. Frank, T. Figy, et al., arXiv:1207.4975 [hep-ph].
- [21] T. Kinoshita, J. Math. Phys. 3 (1962) 650;  
T.D. Lee, M. Nauenberg, Phys. Rev. 133 (1964) B1549.
- [22] Y.L. Dokshitzer, G.D. Leder, S. Moretti, B.R. Webber, J. High Energy Phys. 9708 (1997) 001, arXiv:hep-ph/9707323.
- [23] M. Wobisch, T. Wengler, arXiv:hep-ph/9907280.
- [24] F. Campanario, S. Sapeta, Phys. Lett. B 718 (2012) 100, arXiv:1209.4595 [hep-ph].
- [25] J. Alwall, A. Ballestrero, P. Bartalini, S. Belov, E. Boos, A. Buckley, J.M. Butterworth, L. Dudko, et al., Comput. Phys. Commun. 176 (2007) 300, arXiv:hep-ph/0609017.
- [26] J. Alwall, P. Demin, S. de Visscher, R. Frederix, M. Herquet, F. Maltoni, T. Plehn, D.L. Rainwater, et al., J. High Energy Phys. 0709 (2007) 028, arXiv:0706.2334 [hep-ph].
- [27] C. Oleari, D. Zeppenfeld, Phys. Rev. D 69 (2004) 093004, arXiv:hep-ph/0310156.
- [28] A. Denner, S. Dittmaier, M. Roth, D. Wackeroth, Nucl. Phys. B 560 (1999) 33, arXiv:hep-ph/9904472.
- [29] A.D. Martin, W.J. Stirling, R.S. Thorne, G. Watt, Eur. Phys. J. C 63 (2009) 189, arXiv:0901.0002 [hep-ph].



- [30] M.R. Whalley, D. Bourilkov, R.C. Group, arXiv:hep-ph/0508110.
- [31] M. Cacciari, G.P. Salam, G. Soyez, J. High Energy Phys. 0804 (2008) 063, arXiv:0802.1189 [hep-ph].
- [32] M. Cacciari, G.P. Salam, Phys. Lett. B 641 (2006) 57, arXiv:hep-ph/0512210.
- [33] M. Cacciari, G.P. Salam, G. Soyez, Eur. Phys. J. C 72 (2012) 1896, arXiv:1111.6097 [hep-ph].